Adapted Su-Schrieffer-Heeger Hamiltonian for polypyrrole

Minghai Li and Xi Lin*
Department of Mechanical Engineering and Division of Materials Science and Engineering, Boston University, Boston, Massachusetts 02215, USA
(Received 22 July 2010; published 26 October 2010)

A generic class of Hamiltonians based on the Su-Schrieffer-Heeger (SSH) model is introduced to address the material-specific properties of conducting polymers beyond polyacetylene. Two physical parameters are incorporated into the original SSH model Hamiltonian, one being the scaling parameter γ accounts for the modified electron-phonon coupling strength of aromatic rings and the other parameter ε representing the attractive cores of heterogeneous atoms, such as NH, S, and O. Their values are uniquely determined by two independent measurements, such as the experimental band gap of bulk polypyrrole (PPy) and the dimerization amplitude of pyrrole monomer computed by *ab initio* coupled cluster methods as chosen in this work. With the optimized values of $\{\gamma=1.46, \varepsilon=4.27$ eV$\}$, the adapted SSH (aSSH) Hamiltonian accurately reproduces the band gaps, molecular geometries, quasiparticle energies and wave functions, order parameters, discretized phonons around nonlinear polarons, and infrared and Raman spectra of both neutral and *p*-doped PPy chains of all lengths. It is expected that the generic formalism of the aSSH Hamiltonian, equipped with their corresponding $\{\gamma, \varepsilon\}$ values, would be applicable to other conducting polymers, such as polythiophene, polyfuran, poly-(*p*-phenylene-vinylene), polyaniline, and their functional derivatives.

DOI: 10.1103/PhysRevB.82.155141 PACS number(s): 72.80.Le, 71.38.−k, 72.15.Nj

Conducting polymers based devices have many potential applications, of which the demonstrated examples include organic light-emitting devices,[1] photovoltaic solar cells,[2] field-effect transistors,[3] actuators,[4] supercapacitors and batteries,[5] fuel cell catalysts,[6] gas separation films,[7] and many others.[8] The broad room-temperature electric conductivity spectrum ranging from 10^{-12} to 10^{5} S/cm is the key to all of these fascinating applications. It is recognized that the polymeric electron transport may be understood as various complicated hopping processes of self-localized charge carriers, including the topological solitons, polarons, and bipolarons.[9] These self-localized charge carriers are phonon-dressed electrons and holes which magnify the underlying quasi-one-dimensional (1D) nature of conducting polymers. To capture the essential electron-phonon coupling effects, Su, Schrieffer, and Heeger (SSH) proposed a 1D SSH model Hamiltonian[9–11] whose continuum limit contains one single dimensionless electron-phonon coupling parameter λ.[12,13] A rich variety of intriguing physical phenomena have been demonstrated by using such a simple Hamiltonian and its derivative models, including the Peierls instability,[14–16] reversed spin-charge relation,[9] multiple gap states,[17–19] symmetry-breaking Goldstone mode,[20,21] coupled optical-acoustic distortions,[22,23] attractive soliton and antisoliton pair breather mode,[24] negative spin-density wave,[25,26] three-dimensional (3D) conformational coupling,[27,28] and others.[9] However, because of the lack of explicit specifications of materials properties, this insightful SSH Hamiltonian[9–11] cannot be directly applied to functional conducting polymers beyond their prototypes of *trans*-[10,11] and *cis*-[29] polyacetylene (PA) and therefore limits its applications. In this work, we present a generic class of the adapted SSH (aSSH) Hamiltonians which can accurately model many kinds of conducting polymers by introducing two additional physical parameters, one electron-phonon coupling scaling parameter accounting for the presence of aromatic rings and one on-site energy parameter dealing with the presence of heterogeneous NH, S, and O sites.

As a complementary computational tool, *ab initio* quantum chemical calculations have been widely used to predict many molecular and solid-state materials properties.[30,31] However, the first-principles ground-state density-functional theory (DFT) (Refs. 30, 32, and 33) is known to fail seriously in describing the electronic localization[34,35] of many solid-state systems. This is due to the incorrect convex nature of the energy as the functional of density in the local-density approximation (LDA), so that electrons in solids would inevitably delocalize to lower their ground-state energy.[34] Such an unphysical delocalization tendency makes DFT, an otherwise powerful computational scheme, incompatible for conducting polymers and their applications; and more seriously, the time-dependent DFT (TDDFT) does not perform significantly better due to the intrinsic locality[35] persisting in the adiabatic LDA (ALDA). Therefore, one has to rely on those computationally more extensive methods, such as the time-dependent current DFT,[35] possibly the dynamical mean-field theory,[36] or *ab initio* approaches[31] based on the orbital-dependent potentials in Hartree-Fock (HF),[37,38] hybrid HF-DFT functionals, and post-HF correlation methods,[37,38] as alternative solutions to the localization problem of DFT. Although successful implementations of some of these methods have been demonstrated for conducting polymers, the simple underlying electron-phonon coupling nature is often obscure in these first-principles approaches.

In this work, we describe a generic procedure to construct a physically simple and computationally efficient aSSH Hamiltonian that can deal with a great variety of conducting polymer derivatives, such as polypyrrole (PPy), polythiophene (PT), polyfuran (PFu), poly-(*p*-phenylene-vinylene) (PPV), polyaniline (PANI), and others. Our objective is to provide a set of accurate and efficient computational facilities that were previously unavailable to physicists, chemists, and materials scientists whose main interests

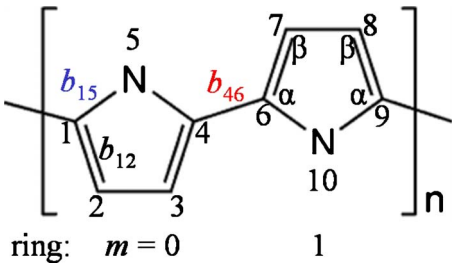

FIG. 1. (Color online) Chemical structure of PPy. The position vector of the ith atomic site is $\mathbf{r}_i$ and the bond length between the ith and jth sites is $b_{ij}=|\mathbf{r}_j-\mathbf{r}_i|$. The α and β carbon sites are the C sites directly connected to the NH sites (such as 1, 4, 6, and 9) and the CH sites two sites away from NH (such as 2, 3, 7, and 8), respectively. The bridge (α-α) bond, such as b_{46}, is the C-C bond that connects two neighboring pyrrole rings via two α-C sites.

are in the fundamental understandings of complicated material-specific properties. In this work, we use PPy to illustrate the general features of the aSSH Hamiltonian; and other conducting polymers are expected to work under identical or similar procedures.

Neutral PPy is a semiconductor with a band gap of 3.2 eV (Refs. 39 and 40) and the room-temperature conductivity of p-doped states can reach 10^3 S/cm.[41] The oxidized PPy films show good mechanical property and excellent chemical stability, therefore they are suitable for various environmental and medical applications.[42] The chemically repeating unit of PPy is an aromatic ring that contains one NH site and four C(H) sites. There are six π electrons per unit ring in neutral PPy, two electrons from the NH site and one from each C(H) site. The ground state of PPy shows the aromatic benzenoid structure. Explicitly, the bond connecting two β-C's is longer than each of the two bonds connecting one α-C and one β-C and the bridge bond that connects two neighboring units is the longest C-C bond. A few 1D SSH models[43,44] have been proposed for PPy, none incorporating these features.

Our aSSH model system have two major components, a regular PA chain consisting of all C(H) sites and individual NH sites chemically bonded to the two α-C sites in every pyrrole unit (Fig. 1). Before detailed specification of the aSSH model, we note that PPy cannot be properly modeled using 1D Hamiltonians because of their implicit 1D constraint. Taking the model shown in Fig. 1 as an example, the implicit 1D constraint requires the bond-length variations satisfying

$$\Delta b_{15}+\Delta b_{45}=\Delta|\mathbf{r}_4-\mathbf{r}_1|=\Delta b_{12}+\Delta b_{23}+\Delta b_{34}, \qquad (1)$$

where $\mathbf{r}_i$ is the position vector of the ith atomic site and $b_{ij}=|\mathbf{r}_j-\mathbf{r}_i|$ is the bond length between the ith and jth sites. Equation (1) implies that the total variation in three C-C bonds must always be equal to the total variation in two C-N bonds in any 1D model Hamiltonians, leading to strongly distorted C-C or C-N bonds. As an instructive comparison, PPV may be properly modeled by 1D Hamiltonians,[45] as long as the two π-conjugation paths through aromatic rings are symmetric given that the phenyl groups are linked at *para*-positions.

Because of the intrinsic flaw in all 1D Hamiltonians, we choose to model PPy using the aSSH Hamiltonian as

$$H_{\mathrm{aSSH}}=\sum_i \frac{1}{2}M_i\dot{\mathbf{r}}_i^2+\sum_{\langle i,j\rangle}-[t_{ij}-\alpha_{ij}(|\mathbf{r}_i-\mathbf{r}_j|-b_{ij}^0)](C_i^+C_j+C_j^+C_i)+\sum_{\langle i,j\rangle}\frac{1}{2}K_{ij}(|\mathbf{r}_i-\mathbf{r}_j|-b_{ij}^0+\delta b_{ij})^2-\varepsilon\sum_m C_m^+C_m. \qquad (2)$$

Here M_i and $\mathbf{r}_i$ are the mass and the position vector of the ith atomic site, respectively. The second and third summations in Eq. (2) run over all the nearest-neighbor (σ-bonded) pairs $\langle i,j\rangle$. The SSH parameters $\{t_{ij},\alpha_{ij},K_{ij}\}$ represent the π-electron hopping integrals of the undimerized configuration, linear π-electron-phonon coupling constant, and σ-bond spring constant, respectively. The original SSH parameters[10,11] are chosen to describe the C-C bonds so that $t_{\mathrm{CC}}=t_0=2.5$ eV, $\alpha_{\mathrm{CC}}=\alpha=4.1$ eV/Å, and $K_{\mathrm{CC}}=K=21$ eV/Å^2 while a different set of the C-N bond parameters $\{t_{\mathrm{CN}},\alpha_{\mathrm{CN}},K_{\mathrm{CN}}\}$ will be discussed in details below. In Eq. (2), the operators C_i and C_i^+ annihilates and creates a π electron on the ith site, respectively. The actual bond length $b_{ij}=|\mathbf{r}_j-\mathbf{r}_i|$ assumes b_{CC}^0 and b_{CN}^0 as the references for C-C and C-N bonds, respectively. As hidden in the original SSH Hamiltonian, b_{CC}^0 and b_{CN}^0 are dummy parameters in the sense that the identical electronic structure and energy and a trivial constant shift of all the bond lengths b_{ij} will be obtained if different bond-length references are chosen; in other words, only the actual bond-length variation Δb_{ij} are physically relevant in Eq. (2). Here we choose to model b_0^{ij} explicitly in order to make direct comparisons to the available experimental and *ab initio* bond lengths. The bond-length contraction amplitude reference δb_{ij} in Eq. (2) is given by the dimerization-coupled analytic expression[23]

$$\delta b_{ij}=-\frac{4\alpha_{ij}}{\pi K_{ij}}\left[1+\frac{1}{2}\left(\ln\frac{z_{ij}}{4}+\frac{3}{2}\right)z_{ij}^2\right], \qquad (3)$$

where $z_{ij}=2\alpha_{ij}A_{ij}/t_{ij}$ and A_{ij} is the local dimerization amplitude;[23] or for simplicity, one may keep only the leading term as the original Su's tensile expression[22]

$$\delta b_{ij}=-\frac{4\alpha_{ij}}{\pi K_{ij}}. \qquad (4)$$

A simple physical interpretation of the $b_{ij}^0-\delta b_{ij}$ reference term is that there is δb_{ij} difference between the equilibrium bond length at which the *pure* σ-bond elastic energy reaches its minimum and the equilibrium bond length at which the σ-bond elastic tensile force is in balance with the intrinsic compressive force of the π-electron hopping. Finally, the last term in Eq. (2) is an ionic Hamiltonian where the creation and annihilation operators C_m^+ and C_m apply *only* on the NH site of the mth pyrrole ring; a positive ε is enforced to attract electrons onto the NH site. For simplicity, we consider in this work only a quasi-two-dimensional (2D) version of Eq. (2),

which explicitly treats the bond-length variations but not the bond bending and twisting angle variations. A complete 3D model Hamiltonian would be necessary if the soliton-coupled bond bending and bond twisting dependences are considered.[27,28]

In the following, we are going to show that the aSSH Hamiltonian of Eq. (2) only requires two extra parameters and their values can be determined by two independent fitting criteria extracted from existing experimental and *ab initio* data. Treating PPy as a linear PA chain with periodic NH side groups, we keep the C-C bond parameters as the original SSH values.[10,11] For the C-N bonds, we argue that both the dimensionless phonon-electron coupling $\lambda \equiv \frac{2\alpha^2}{\pi K t_0}$ and the effective σ-bond spring constant K should be the same as those for the C-C bonds. One may understand the argument from the band-gap perspective; namely, $E_g = 2\Delta_0 = \frac{16t_0}{e} e^{-1/2\lambda}$ is unlikely to change exponentially only because CH is replaced by NH or the formation of aromatic rings. So we choose $\{t_{CN} = \gamma t_0, \alpha_{CN} = \sqrt{\gamma}\alpha_0, K_{CN} = K_0\}$, where γ is an electron-phonon scaling parameter. Since δb_{ij} are given by either Eq. (3) or Eq. (4) and b_0^{ij} are essentially dummy parameters, we are left with two physical parameters $\{\gamma, \varepsilon\}$, in which the electron-phonon scaling parameter γ takes care of the difference between C-N bonds (which close aromatic rings) and C-C bonds and the on-site energy parameter ε describes the difference between NH sites and C(H) sites. As a side note, our numeric calculations also indicate that when the on-site parameter ε is fixed, virtually identical bond-length configurations and electronic structures are found even with a different choice of the parameters $\{\gamma t_0, \gamma\alpha_0, \gamma K_0\}$.

In t-PA, the fundamental band gap $E_g = 2\Delta_0 = \frac{16t_0}{e} e^{-1/2\lambda}$ determines all the other major physical properties, in particular, the dimerization amplitude $4u_0 = \frac{\Delta_0}{\alpha}$ and the soliton width $2\xi = \frac{4t_0 a}{\Delta_0}$.[9,13] In PPy, the presence of NH sites as well as the aromatic rings decouples these fundamental relations, which allows us to choose the band gap and the dimerization amplitude as two independent fitting criteria for the parameter set $\{\gamma, \varepsilon\}$.

The π-π^* band gap for a neutral finite N-Py chain, where N is the number of pyrrole rings, is conveniently defined as the energy difference between the lowest unoccupied molecular orbital (LUMO) and the highest occupied molecular orbital (HOMO) $E_g(N) = E_{LUMO}(N) - E_{HOMO}(N)$. The bond-length dimerization amplitude is measured by $\Delta b_{\beta\beta-\alpha\beta}(N) = b_{\beta\beta} - \bar{b}_{\alpha\beta}$, where $b_{\beta\beta}$ is the C_β-C_β bond length and $\bar{b}_{\alpha\beta}$ is the average length of the two C_α-C_β bonds in the central Py ring of the N-PPy chain, so that positive $\Delta b_{\beta\beta-\alpha\beta}$ values imply aromatic structures and negative values imply quinoid structures. It is obvious that both $E_g(N)$ and $\Delta b_{\beta\beta-\alpha\beta}(N)$ may vary significantly for small values of N. The variations with N are consequences of the finite size effect, due to the discreteness of electronic energy levels and the chain termination condition, such as the open or closed chains. Both effects should vanish when N is large.

A systemic study of $E_g(N)$, corresponding to the peaks in the ultraviolet-visible absorption spectra of the corresponding neutral N-Py oligomers, gave $E_g(7) = 3.25$ eV by Zotti *et al.*[40] This value is close to $E_g = 3.2$ eV for electrochemically deposited PPy films of unspecified chain lengths using the normalized differential conductance spectra by Yang *et al.*[39] Computationally, it is well known that the HF quasiparticle energy spectrum seriously overestimates the band gap for virtually all materials, and the DFT quasiparticle energy spectrum does the opposite.[34] We thus choose the experimentally measured values for our $\{\gamma, \varepsilon\}$ parameter fitting. The band-gap optimization results are shown Fig. 2(a), an energy contour with respect to $\{\gamma, \varepsilon\}$. From Fig. 2(a), one sees that small scaling parameters γ and large on-site parameters ε generally lead to small band gaps E_g, and *vice versa.* It is interesting to note that for a given E_g, there exists a corresponding minimal threshold $\{\gamma_{min}, \varepsilon_{min}\}$ so that no solutions below such a threshold value would be allowed; for instance, the threshold for $E_g(7) = 4.07$ eV is $\{\gamma_{min} = 1.65, \varepsilon_{min} = 3.40$ eV$\}$, shown as the triangle in Fig. 2(a). For parameter values that are above the threshold, the scaling parameter γ may assume two different values for any fixed $\varepsilon > \varepsilon_{min}$ and E_g. To the main interest of this work, the fitting target $E_g(7) = 3.25$ eV is highlighted as the pluses in Fig. 2(a).

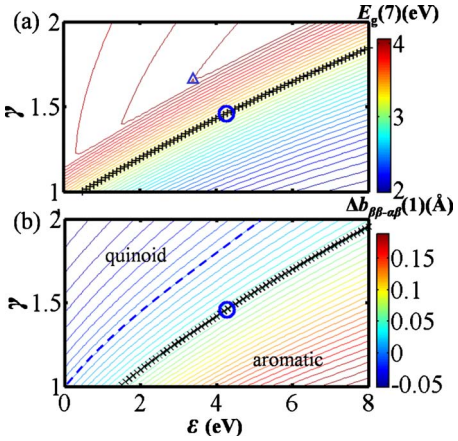

FIG. 2. (Color online) The band gap E_g and bond-length dimerization amplitude $\Delta b_{\alpha\beta-\beta\beta}$ as functions of the electron-phonon scaling parameters γ and the NH on-site energy parameter ε. (a) Contour plot of E_g for $N=7$, with the pluses indicating the targeted experimental value $E_g = 3.25$ eV. (b) Contour plot of $\Delta b_{\beta\beta-\alpha\beta}$ for $N=1$, with the crosses indicating the CCSD result of $\Delta b_{\beta\beta-\alpha\beta} = 0.051$ Å. The optimized parameter set $\{\gamma = 1.46, \varepsilon = 4.27$ eV$\}$ which gives $\{E_g = 3.25$ eV, $\Delta b_{\beta\beta-\alpha\beta} = 0.051$ Å$\}$ is highlighted as the circles in both (a) and (b). The dashed line in (b), $\Delta b_{\beta\beta-\alpha\beta} = 0$ Å, indicates the phase boundary of the quinoid and aromatic structures.

The experimentally measured $\Delta b_{\beta\beta-\alpha\beta}(N)$ varies significantly, ranging from $\Delta b_{\beta\beta-\alpha\beta}(1) = 0.043$, 0.043, 0.058, 0.036, 0.079, and 0.064 Å depending on the six possible models proposed by Bak *et al.* using deuterated pyrrole microwave spectra,[46] $\Delta b_{\beta\beta-\alpha\beta}(1) = 0.035$ Å as listed on the NIST website[47] using microwave spectra, $[\Delta b_{\beta\beta-\alpha\beta}(2) + \Delta b_{\beta\beta-\alpha\beta}(3)]/2 = 0.045$ Å based on an unpublished x-ray data by Street and Nazzal, cited as Ref. 16 in the work by Andre *et al.*,[48] to $\Delta b_{\beta\beta-\alpha\beta}(3) = 0.052$ Å based on an unpublished experimental data by Street and Nazzal, cited as Ref. 22 in the work by Bredas *et al.*[49] In contrast, the post-HF correlation methods such as the coupled cluster with single and double substitutions (CCSD) and the quadratic configu-

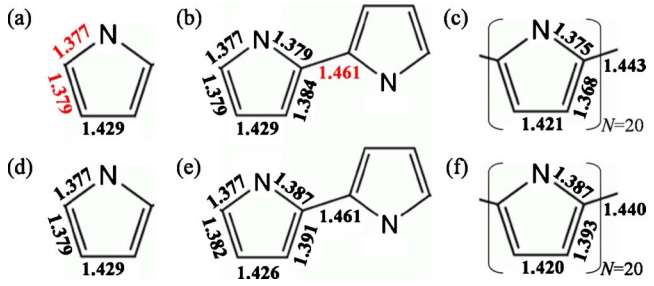

FIG. 3. (Color online) Bond lengths of the (a) pyrrole monomer and (b) dimer computed by CCSD and the $N=20$ oligomer (shown only the central ring) (c) computed by HF. Bond lengths of the pyrrole (d) monomer, (e) dimer, and $N=20$ oligomer (shown only the central ring) (f) computed by the aSSH Hamiltonian. The three bond-length fitting targets, obtained by CCSD, are highlighted in red bold. All bond lengths are in angstrom. The basis sets for CCSD and HF are 6-31++G(d,p) and 3-21G, respectively.

ration interaction with single and double substitutions (QCISD) (Ref. 50) gave the same $\Delta b_{\beta\beta-\alpha\beta}(1)=0.051$ Å. Despite apparent numeric differences, all these experimental and computational results conclude that neutral N-PPy oligomers contain only aromatic rings. Based on the overall quality of these data, we choose $\Delta b_{\beta\beta-\alpha\beta}(1)=0.051$ Å as our parameter fitting target. The aSSH Hamiltonian results on $\Delta b_{\beta\beta-\alpha\beta}$ are shown in Fig. 2(b), with the crosses indicating the target $\Delta b_{\beta\beta-\alpha\beta}(1)=0.051$ Å. The crossing point of pluses in Fig. 2(a) and crosses in Fig. 2(b) finds the optimized parameter set $\{\gamma=1.46,\varepsilon=4.27$ eV$\}$, which will be used in the rest of the paper. With the two contour plots of Figs. 2(a) and 2(b), one may find the optimized parameter values for other $\{E_g,\Delta b_{\beta\beta-\alpha\beta}\}$ targets. For example, $\{E_g(7)=3.25$ eV$,\Delta b_{\beta\beta-\alpha\beta}(1)=0.045$ Å$\}$ finds the corresponding optimal parameter set of $\{\gamma=1.36,\varepsilon=3.40$ eV$\}$. Finally, we note that the dashed line in Fig. 2(b) is the phase boundary separating the quinoid structure for large γ and small ε from the aromatic structure for small γ and large ε. The quinoid region in Fig. 2(b) corresponds to the flat E_g region in Fig. 2(a), implying that E_g of quinoid structures is less sensitive to γ and ε compared to E_g of aromatic structures.

With the optimal parameter set $\{\gamma=1.46,\varepsilon=4.27$ eV$\}$, the bond-length references b_{CC}^0 and b_{CN}^0 may be determined by using existing experimental or *ab initio* data. Explicitly, choosing the absolute bond lengths of the pyrrole monomer computed by CCSD, $b_{\alpha\beta}(1)=1.379$ Å and $b_{\mathrm{CN}}(1)=1.377$ Å as the fitting targets [Fig. 3(a)], we obtain $b_{\mathrm{CC}}^0=1.662$ Å and $b_{\mathrm{CN}}^0=1.637$ Å for the aSSH Hamiltonian. Finally, since the bridge bond that connects the two adjacent pyrrole units does not participate in any aromatic rings, a different bond-length reference $b_{\alpha\alpha}^0$ may be used. Taking the bond-length reference of $b_{\alpha\alpha}(2)=1.461$ Å [Fig. 3(b)] computed by CCSD for the pyrrole dimer, we find $b_{\alpha\alpha}^0=1.556$ Å. The aSSH results of the pyrrole monomer and dimer are summarized in Figs. 3(d) and 3(e), respectively. Again, we note that these reference bond lengths are relevant only to obtain the absolute bond lengths, and they do not have any effects on the underlying electronic structures.

With $\{\gamma=1.46,\varepsilon=4.27$ eV$\}$, we compute E_g for a serial of neutral PPy chains that contain N monomers, with

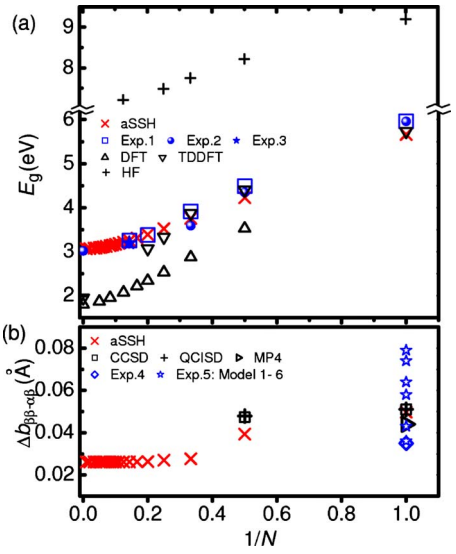

FIG. 4. (Color online) The quasiparticle energy band gap E_g and the bond-length dimerization amplitude $\Delta b_{\beta\beta-\alpha\beta}$ of PPy as a function of N computed by the aSSH model with $\{\gamma=1.46,\varepsilon=4.27$ eV$\}$. The DFT, TDDFT, and experimental data 1–5 are taken from Refs. 51, 52, 40, 53, and 39 ($E_g=3.2$ eV with an unknown N, assumed to be 7), Refs. 47 and 46, respectively. The HF, CCSD, QCISD, and MP4 are computed using GAUSSIAN-03 (Ref. 37) with the 6-31++G(d,p) basis set.

$N=1,2,3,\ldots,25,30,50,$ and 100 using the aSSH Hamiltonian. The results are shown in Fig. 4, plotted against available experimental data,[39,40] *ab initio* HF, and first-principles DFT (Ref. 51) and TDDFT (Ref. 52) calculations. With the only fitted date point of $E_g(7)=3.25$ eV, our aSSH results (red crosses) match closely with all the ultraviolet-visible adsorption data measured by Zotti *et al.*[40] and by Diaz *et al.*[53] and with the normalized differential conductance spectra measured by Yang *et al.*[39] on electrochemically deposited PPy films of unspecified chain lengths [$N=7$ is used in Fig. 4(a)]. In contrast, systematic overestimations and underestimations of $E_g(N)$ are found in HF and DFT calculations, respectively. TDDFT performs well for small oligomers of $N<5$ (Ref. 35) but nevertheless converges to the ground-state DFT results at the long-chain limit due to the ALDA approximation. The bond-length alternation amplitude $\Delta b_{\beta\beta-\alpha\beta}(N)$ is plotted as a function of N in Fig. 4(b), which shows a faster convergence than $E_g(N)$ in the large N limit. All the aSSH ground states show the benzenoid configuration. Besides the pyrrole monomer and dimer cases discussed above, the configurations of long-chain oligomers computed by the aSSH Hamiltonian also agree well with the HF results. Figure 3(f) shows a central ring configuration of the $N=20$ oligomer. Among all the bond lengths, the largest deviation is 2.5% at the $b_{\alpha\beta}$ bond, which is mainly caused by the overestimation of the dimerization amplitude in HF results.

Furthermore, the aSSH quasiparticle energies, density of states (DOS), and wave functions of the $N=1$ [Fig. 5(a)], $N=2$ [Fig. 5(b)], and $N=20$ [Fig. 5(c)] PPy chains can accurately reproduce all the corresponding *ab initio* HF quasiparticle results despite that HF overestimates the band gap.

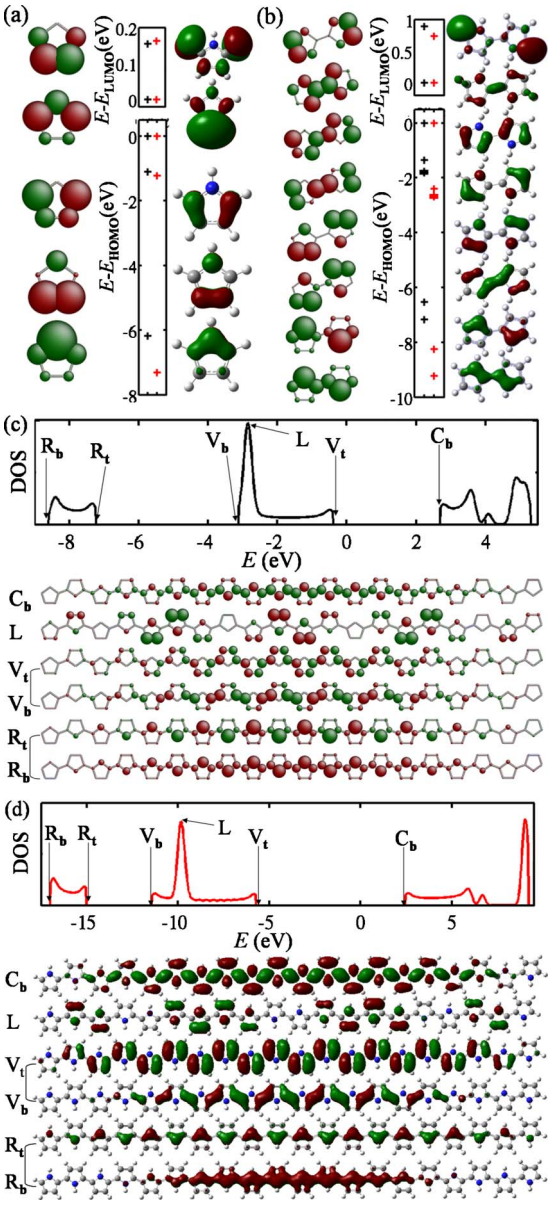

FIG. 5. (Color online) The complete sets of filled and subsets of unfilled π orbitals of the neutral PPy of (a) $N=1$, (b) $N=2$, and $N=20$ (c) for aSSH and (d) for HF. In (a) and (b), the aSSH results are shown on the left and HF results on the right, with the aSSH $E_{\mathrm{HOMO}}(N=1)=-1.69$ eV, $E_{\mathrm{LUMO}}(N=1)=3.97$ eV, $E_{\mathrm{HOMO}}(N=2)=-1.04$ eV, and $E_{\mathrm{LUMO}}(N=2)=3.18$ eV and the HF $E_{\mathrm{HOMO}}(N=1)=-8.16$ eV, $E_{\mathrm{LUMO}}(N=1)=4.14$ eV, $E_{\mathrm{HOMO}}(N=2)=-7.02$ eV, and $E_{\mathrm{LUMO}}(N=2)=2.99$ eV. The red and green wave function lobes represent two different phases of the corresponding quasiparticle wave functions and their sizes are proportional to the wave-function amplitudes on the corresponding atomic sites. The HF wave function isosurface values are 0.8 $\text{Å}^{-3/2}$, 0.6 $\text{Å}^{-3/2}$, and 0.2 $\text{Å}^{-3/2}$ for the monomer, dimer, and $N=20$ cases, respectively. For HF results, the 6-31G++(d,p) basis set is used for monomer and dimer, and the 3-21G basis sets for $N=20$.

Compared to t-PA described by the conventional SSH Hamiltonian,[9–11] the PPy band structure displays two new features: a low-lying pyrrole ring band (Fig. 5, R_b and R_t representing the states at the bottom and top of this band,

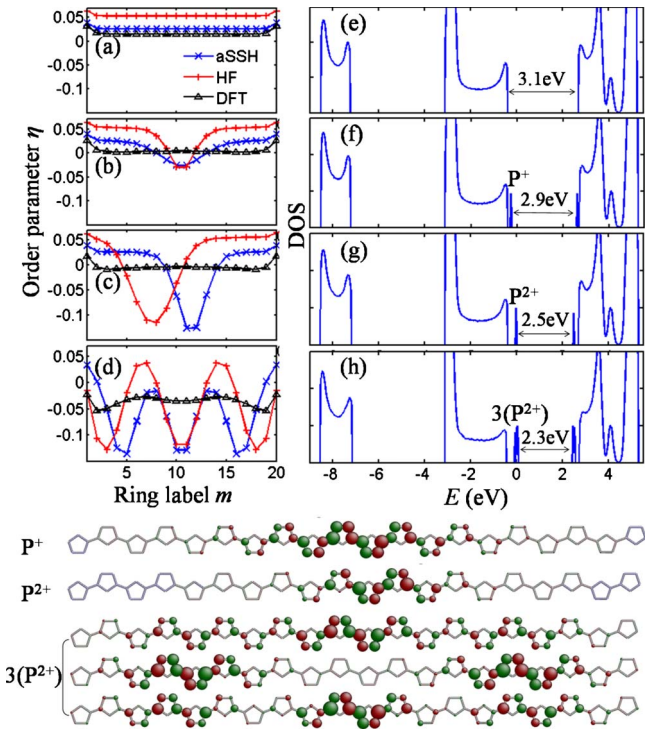

FIG. 6. (Color online) The bond-length alternation order parameter (a)–(d) $\eta(m)$, (e)–(h) DOS, and the corresponding polaron wave functions of an $N=20$ PPy chain computed by the aSSH Hamiltonian. (a) and (e) are the neutral $N=20$ PPy reference. (b) and (f) contain one polaron P^+. (c) and (g) contain one bipolaron P^{2+}. A bipolaron lattice, $3(P^{2+})$, starts to form above 30% doping, (d) and (h). The order parameters computed by DFT-PBE and HF, both using the 3-21G basis set in GAUSSIAN-03 (Ref. 37), are shown as delocalization versus localization comparisons.

respectively) and the localized band (Fig. 5, represented by L) that overlaps in energy with the delocalized valence band (Fig. 5, V_b and V_t representing the states at the bottom and top of the band, respectively). The ring band is formed by the bonding and antibonding combinations of the monomer ground state [Fig. 5(a)]. The localized L states are the complete bonding and antibonding combinations of the second-lowest state of the monomer whose wave function has two nodes precisely located at the two bridge C atoms [Fig. 5(a)]. Such a nodal structure effectively decouples every pyrrole unit from the rest of the chain so that its band state energy is the same as the isolated monomer case. In other words, the energy of the L band is flat in the reciprocal space similar to the PPV case.[45] One notable difference between the aSSH and HF DOS results is that HF has a broader valence band, which can be seen in Fig. 5(d) from the energy difference between the V_b and L states. Since PPy can only be p-doped, the wave functions above LUMOs are not explicitly shown in Fig. 5(c) and 5(d).

Upon p-doping, self-localized polarons are formed due to the strong 1D electron-phonon coupling. From the phonon perspective, the bond-length alternation order parameter, defined as $\eta(m)=b_{\beta\beta}(m)-\bar{b}_{\alpha\beta}(m)$, where m is the ring label (Fig. 1) and $\bar{b}_{\alpha\beta}$ is the average length of the two C_α-C_β bonds, displaces a transition from the aromatic to quinoid

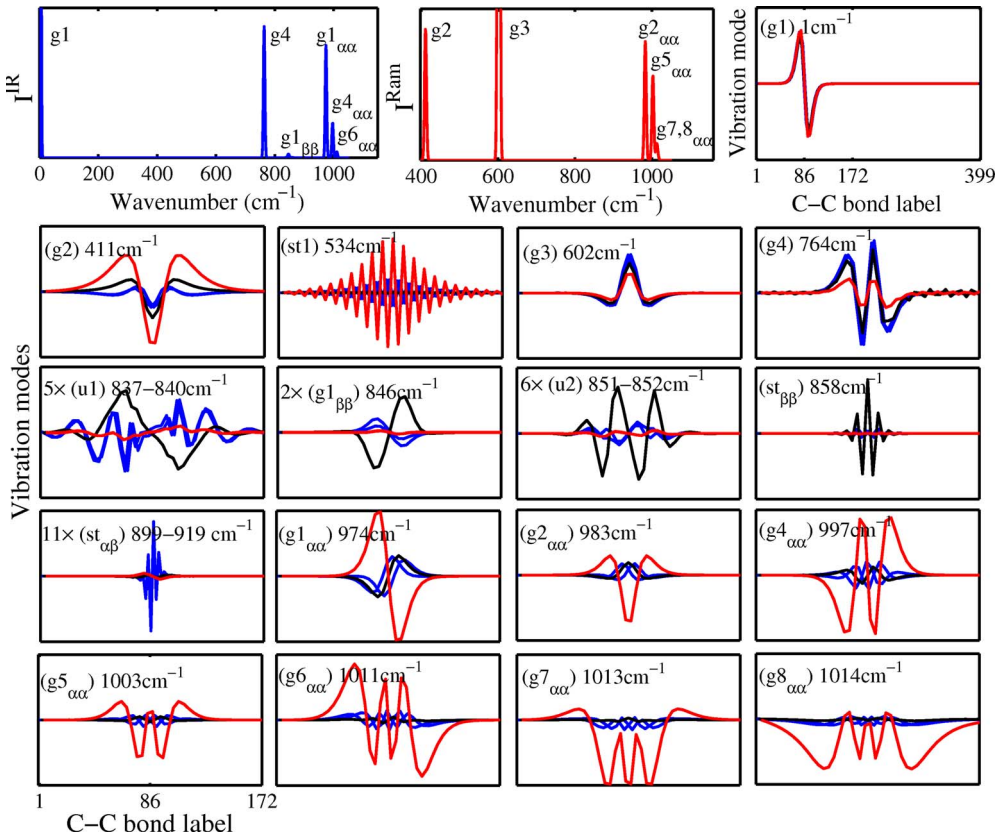

FIG. 7. (Color online) The first-order IR intensity I^{IR}, Raman-scattering activity I^{Ram}, and the 37 (or 17 nondegenerate) localized C-C vibrational modes $Q_k(i)=(-1)^i\Delta b_i$ are plotted for an $N=100$ PPy chain, where i labels the number order of C-C bonds. Explicitly, the bond pairs of $\langle 5m+1,5m+2\rangle$, $\langle 5m+2,5m+3\rangle$, $\langle 5m+3,5m+4\rangle$, and $\langle 5m+4,5m+6\rangle$ defined by Fig. 1 are labeled as the bonds of number $4m+1$, $4m+2$, $4m+3$, and $4m+4$, respectively; Δb_i measures the change in the ith C-C bond length according to the vibrational mode Q_k. No differences in the IR or Raman spectra are found for $N=20$; however the $N=100$ vibrational modes show clearer localizations. Only the localized regions are plotted for all the vibrational modes except for the Goldstone mode g1. The vibrational mode indices are labeled according to the primary motions; for instance, $2\times(\mathrm{g1}_{\beta\beta})846\ \mathrm{cm}^{-1}$ indicates that this mode is the g1 mode involving primarily β-β bonds with a vibrational frequency of 846 cm^{-1} and the degeneracy is 2. Vibrational modes are plotted in colors, red for α-α (bridge) bonds, blue for α-β and β-α bonds, and black for β-β bonds.

structures [Figs. 6(b)–6(d)]. Since DFT underestimates and HF overestimates the band gap E_g, their corresponding order parameters are too much delocalized and too much localized, respectively. From the electron perspective, polarons and bipolarons are gap states existing in the forbidden band gap [Figs. 6(e)–6(h)] so that they have characteristic exponential decaying wave-function tails. Explicitly, the soliton (and antisoliton) half width of the polaron P^+ and bipolaron P^{2+} are found to be 2.7 and 1.6 Py rings, respectively, which correctly reflects that fact that the P^{2+} state [Fig. 6(g)] is closer to the band-gap center than the P^+ state [Fig. 6(f)]. However, a bipolaron P^{2+} may still occupy more carbon sites than a polaron P^+, as long as the distance between the soliton center and the antisoliton center of a bipolaron P^{2+} is much larger than the corresponding distance of a polaron P^+. The fact that the aSSH bipolaron P^{2+} occupies less carbon sites than the aSSH polaron P^+ as shown in Fig. 6 is because the self-energies[54] of the noninteracting aSSH quasiparticles are precisely zero; the missing electron-electron correlations may be restored via the on-site and off-site Hubbard and extended-Hubbard terms.[19,23,25] Moreover, we note that an isolated polaron P^+ or bipolaron P^{2+} shown in Fig. 6 seem to favor the chain center is a finite ($N=20$) chain length effect. For a much longer chain ($N=100$, Fig. 7), the aSSH result indicates that the soliton and antisoliton centers of an isolated polaron P^+ always energetically favor the bridge bonds and the overall polaron P^+ center is 22 Py rings away from one of the chain edges. Such a polaron-edge attraction in PPy is opposite to the t-PA case, in which an isolated soliton, polaron, or bipolaron always favors the chain center.[55]

The discretized linear modes[56,57] around nonlinear polaron P^+ and their corresponding infrared (IR) and Raman spectra of an $N=100$ PPy chain are shown in Fig. 7. The linear modes are computed by diagonalizing the mass-weighted force-constant matrix $\frac{\partial^2 E_{\mathrm{aSSH}}}{\sqrt{M_i M_j}\partial x_{i,p}\partial x_{j,q}}$, where E_{aSSH} is the total energy of the aSSH Hamiltonian and $x_{i,p}$ represents the ith atom in the pth dimension (x, y, and z). In our current quasi-2D bond-length implementation, a total of 599 independent (C-C and C-N) bond modes are found for the $N=100$ PPy chain. Figure 7 shows all the 17 nondegenerate localized modes.[56,57] The IR-active Goldstone mode g1 (at $\sim 0\ \mathrm{cm}^{-1}$) is the translational motion of the polaron, similar to the t-PA case.[58] This mode is in sharp contrast to three new out-of-phase translational modes, the doubly degenerate

$g1_{\beta\beta}$ modes (at 846 cm^{-1}) where the dominant β-β bonds (black) are in the opposite phase as the α-β and β-α bonds (blue) while keeping the α-α (bridge) bonds still (red) and the $g1_{\alpha\alpha}$ mode (at 974 cm^{-1}) where the dominant α-α (bridge) bonds (red) are in the opposite phase as the rest of bonds. Similarly, both in- and out-of-phases are present in the amplitude oscillation (g2) modes[56,57] and the staggered (st1) modes.[58] In addition, there are five unknown modes (u1) at 837–840 cm^{-1} and six unknown modes (u2) at 851–852 cm^{-1}; these modes have weak IR and Raman responses.

Under the linear dipole moment approximation, the IR intensity I_k^{IR} is proportional to the square of the derivative of the dipole moment P with respect to the associated normal coordinate Q_k; namely, $I_k^{\mathrm{IR}} \propto \left|\frac{\partial P}{\partial Q_k}\right|^2$.[59] The IR intensity ratios shown in Fig. 7 are found to be $g1:g4:g1_{\alpha\alpha}:g4_{\alpha\alpha}:g6_{\alpha\alpha}:g1_{\beta\beta}=953:36:31:10:1.6:1$. The Raman-scattering activity of Q_k defined as $I_k^{\mathrm{Ram}}=45\alpha'^2+7\beta'^2$, where α' and β' are the mean polarizability derivative and the anisotropy polarizability tensor derivative, respectively.[59] These polarizability derivatives are numerically evaluated using the finite-field approach.[60] The Raman-scattering activity ratios shown in Fig. 7 are found to be $g3:g2_{\alpha\alpha}:g5_{\alpha\alpha}:g7_{\alpha\alpha}:g8_{\alpha\alpha}=298:24:22:15:2.2:1$. Although only π-electron contributions are explicitly computed in the aSSH model, we expect the localized modes and IR and Raman spectra shown in Fig. 7 representing the doping-induced vibrational activity changes. With additional external Coulomb trapping potentials as implemented in the amplitude mode formalism[61] by counter ions and the interchain exciton approach,[62] the aSSH Goldstone mode frequency can be lifted to be a finite value so that direct experimental comparisons would be more appropriate. Detailed implementation of the external Coulomb trapping potential is beyond the scope of this work and will be presented separately.

In summary, we propose in this work an aSSH model Hamiltonian that is able to accurately describe many fundamental properties of neutral and doped PPy chains of any length, including the band gaps, bond-length alternating amplitudes, molecular geometries, order parameters, DOS, quasiparticle wave functions, linear phonons around nonlinear self-localized charge carriers, and IR and Raman spectra. These results reveal one sensible although previously hidden physics; namely, the fundamental difference between t-PA and other conducting polymers is indeed physically simple, requiring merely an electron-phonon scaling parameter γ and a heterogeneous on-site parameter ε. The two transferable physical parameters demonstrated in this work for PPy should be applicable to model PT and PFu (both using the identical Fig. 2), PPV, PANI, and porphyrin. To be coupled with a proper description of interchain interactions, and if necessary the near-neighbor Hubbard terms for correlation effects, the aSSH model may offer an accurate and efficient computational tool to fundamentally understand disordered charge transport processes of conducting polymers.

The authors acknowledged thoughtful discussions with Sidney Yip, Kazuhiro Kagawa, and Boku Sen. This work was supported by Honda R&D Co., Ltd, Idaho National Laboratory, and NSF TeraGrid under Grant No. DMR-090073.

*Author to whom all correspondence should be addressed; linx@bu.edu

[1] J. H. Burroughes, C. A. Jones, and R. H. Friend, Nature (London) **335**, 137 (1988).
[2] N. S. Sariciftci, L. Smilowitz, A. J. Heeger, and F. Wudl, Science **258**, 1474 (1992).
[3] F. Garnier, R. Hajlaoui, A. Yassar, and P. Srivastava, Science **265**, 1684 (1994).
[4] E. Smela, O. Inganäs, and I. Lundström, Science **268**, 1735 (1995).
[5] S. Roth and D. Carroll, *One-Dimensional Metals* (Wiley-VCH, Weinheim, 2004).
[6] R. Bashyam and P. Zelenay, Nature (London) **443**, 63 (2006).
[7] M. R. Anderson, B. R. Mattes, H. Reiss, and R. B. Kaner, Science **252**, 1412 (1991).
[8] T. A. Skotheim and J. R. Reynolds, *Handbook of Conducting Polymers* (Taylor & Francis, Boca Raton, 2007).
[9] A. J. Heeger, S. Kivelson, J. R. Schrieffer, and W.-P. Su, Rev. Mod. Phys. **60**, 781 (1988).
[10] W. P. Su, J. R. Schrieffer, and A. J. Heeger, Phys. Rev. Lett. **42**, 1698 (1979).
[11] W. P. Su, J. R. Schrieffer, and A. J. Heeger, Phys. Rev. B **22**, 2099 (1980).
[12] H. Takayama, Y. R. Lin-Liu, and K. Maki, Phys. Rev. B **21**, 2388 (1980).
[13] E. M. Conwell, IEEE Transactions on Electrical Insulation **EI-22**, 591 (1987).
[14] S. Kivelson and D. E. Heim, Phys. Rev. B **26**, 4278 (1982).
[15] J. E. Hirsch, Phys. Rev. Lett. **51**, 296 (1983).
[16] D. K. Campbell, T. A. DeGrand, and S. Mazumdar, Phys. Rev. Lett. **52**, 1717 (1984).
[17] J. Orenstein and G. L. Baker, Phys. Rev. Lett. **49**, 1043 (1982).
[18] X. Wei, B. C. Hess, Z. V. Vardeny, and F. Wudl, Phys. Rev. Lett. **68**, 666 (1992).
[19] X. Lin, J. Li, C. J. Först, and S. Yip, Proc. Natl. Acad. Sci. U.S.A. **103**, 8943 (2006).
[20] H. Ito and A. Terai, J. Phys. Soc. Jpn. **53**, 3520 (1984).
[21] E. J. Mele and M. J. Rice, Phys. Rev. Lett. **45**, 926 (1980).
[22] W. P. Su, Solid State Commun. **35**, 899 (1980).
[23] M. Li and X. Lin, Phys. Rev. B **81**, 153102 (2010).
[24] A. R. Bishop, D. K. Campbell, P. S. Lomdahl, B. Horovitz, and S. R. Phillpot, Phys. Rev. Lett. **52**, 671 (1984).
[25] K. R. Subbaswamy and M. Grabowski, Phys. Rev. B **24**, 2168 (1981).
[26] L. M. Tolbert and M. E. Ogle, J. Am. Chem. Soc. **111**, 5958 (1989).
[27] X. Lin, J. Li, and S. Yip, Phys. Rev. Lett. **95**, 198303 (2005).
[28] X. Lin, J. Li, E. Smela, and S. Yip, Int. J. Quantum Chem. **102**, 980 (2005).
[29] S. A. Brazovskii and N. N. Kirova, JETP Lett. **33**, 4 (1981).

[30] W. Kohn, Rev. Mod. Phys. **71**, 1253 (1999).
[31] J. A. Pople, Rev. Mod. Phys. **71**, 1267 (1999).
[32] http://cms.mpi.univie.ac.at/vasp/
[33] http://www.abinit.org/
[34] A. J. Cohen, P. Mori-Sanchez, and W. Yang, Science **321**, 792 (2008).
[35] M. van Faassen, P. L. de Boeij, R. van Leeuwen, J. A. Berger, and J. G. Snijders, Phys. Rev. Lett. **88**, 186401 (2002).
[36] G. Kotliar, S. Y. Savrasov, K. Haule, V. S. Oudovenko, O. Parcollet, and C. A. Marianetti, Rev. Mod. Phys. **78**, 865 (2006).
[37] http://www.gaussian.com
[38] http://www.emsl.pnl.gov/docs/nwchem/nwchem.html
[39] R. Yang, W. H. Smyrl, D. F. Evans, and W. A. Hendrickson, J. Phys. Chem. **96**, 1428 (1992).
[40] G. Zotti, S. Martina, G. Wegner, and A.-D. Schlüter Adv. Mater. **4**, 798 (1992).
[41] A. B. Kaiser, Rep. Prog. Phys. **64**, 1 (2001).
[42] E. Smela, Adv. Mater. **15**, 481 (2003).
[43] N. A. de Brito and M. G. e Silva, Int. J. Quantum Chem. **103**, 604 (2005).
[44] Y. Yuan, T. F. George, and X. Sun, Commun. Theor. Phys. **48**, 366 (2007).
[45] N. Kirova, S. Brazovskii, and A. R. Bishop, Synth. Met. **100**, 29 (1999).
[46] B. Bak, D. Christensen, L. Hansen, and J. Rastrup-Andersen, J. Chem. Phys. **24**, 720 (1956).
[47] http://cccbdb.nist.gov/
[48] J. M. André, D. P. Vercauteren, G. B. Street, and J. L. Brédas, J. Chem. Phys. **80**, 5643 (1984).
[49] J. L. Brédas, B. Thémans, J. G. Fripiat, J. M. André, and R. R. Chance, Phys. Rev. B **29**, 6761 (1984).
[50] M. J. Frisch *et al.*, Gaussian, Inc., Pittsburgh, PA, 2003.
[51] G. R. Hutchison, Y. J. Zhao, B. Delley, A. J. Freeman, M. A. Ratner, and T. J. Marks, Phys. Rev. B **68**, 035204 (2003).
[52] J. Ma, S. Li, and Y. Jiang, Macromolecules **35**, 1109 (2002).
[53] A. F. Diaz, J. Crowley, J. Bargon, G. P. Gardini, and J. B. Torrance, J. Electroanal. Chem. Interfacial Electrochem. **121**, 355 (1981).
[54] R. D. Mattuck, *A Guide to Feynman Diagrams in the Many-Body Problem* (McGraw-Hill, New York, 1976).
[55] Y. Shin, M. Li, A. L. Botelho, and X. Lin (unpublished).
[56] J. Goldstone and R. Jackiw, Phys. Rev. D **11**, 1486 (1975).
[57] Y. Wada and J. R. Schrieffer, Phys. Rev. B **18**, 3897 (1978).
[58] A. Terai, H. Ito, Y. Ono, and Y. Wada, J. Phys. Soc. Jpn. **54**, 196 (1985).
[59] D. Porezag and M. R. Pederson, Phys. Rev. B **54**, 7830 (1996).
[60] J. L. Bredas, C. Adant, P. Tackx, A. Persoons, and B. M. Pierce, Chem. Rev. **94**, 243 (1994).
[61] B. Horovitz, Solid State Commun. **41**, 729 (1982).
[62] W. P. Su, Phys. Rev. B **35**, 9245 (1987).